



The Elastic and Inelastic Post-Buckling Behavior of Steel Plate Shear Wall Web Plates and their Interaction with Vertical Boundary Elements

D.J. Webster¹, J.W. Berman², L.N.Lowes³

Abstract

The Special Plate Shear Wall, or SPSW, is a building lateral system that relies primarily on the in-plane post-buckling strength and stiffness of thin steel plates. SPSWs have been utilized as a building lateral system since the 1960's. Many numerical and experimental studies have been undertaken to investigate the behavior of the complete SPSW system, including the interaction of the web plates and the surrounding boundary frame, but few studies have attempted to isolate the behavior of the steel web plate alone.

As a thin metal plate is loaded in shear beyond its critical buckling stress, the majority of the applied load is resisted by tension-field action. The conventional assumption is that the compressive stress remains at the critical stress magnitude after the plate buckles. This critical stress is usually very low for a normally proportioned SPSW, and is a very small fraction of the plate yield stress. Consequently its contribution is typically ignored.

This paper presents the results of continuum shell element analyses on SPSW sub-assemblies loaded in shear and bending. The results suggest that after buckling the average compressive stress may significantly exceed the critical buckling stress, and may exceed 20% of the simultaneous average principal tensile stress. A review of past experimental results indicate that the flexural demands on the vertical boundary elements is often lower than that obtained using the tension-only strip element model - the conventional design approach. A possible explanation is the presence of principal compressive stresses that act concurrently with the tension field. The reduced boundary member demand is also observed in the shell element models.

1. Introduction and SPSW Primer

There are two primary components of a SPSW: 1) A boundary frame, typically a single bay multi-story moment frame, typically consisting of wide flange (WF) section beams and columns; and 2) unreinforced steel panels (web plates) which are welded or bolted into the space formed by the beams and columns via a continuous steel tab (fish plate). The beams in a SPSW are

¹ Graduate Research Assistant., University of Washington, djw39@u.washington.edu

² Assistant Professor, University of Washington, jwberman@u.washington.edu

³ Associate Professor, University of Washington, lowes@u.washington.edu

referred to as horizontal boundary elements (HBEs) and the columns as vertical boundary elements (VBEs). The HBEs are typically moment connected to the VBEs with detailing similar to special moment resisting frame (SMRF) or intermediate moment resisting frame (IMRF) connections. This is a system requirement in US building codes for SPSWs designed for ductile seismic response. The web plates in a SPSW are relatively thin and made from mild steel sheet or plate. The length to thickness ratio (L/t) of a panel varies with demand but may be in the range 300 to 2000. This results in a web plate thickness that may range from 1 mm to over 25 mm for a high-rise structure.

1.1 SPSW System Behavior

The behavior of SPSWs is perhaps not as well understood as other commonly used systems, such as concentrically braced frames, as there are a limited number of buildings with SPSW lateral systems that have been subjected to large earthquakes. Consequently, there is limited data available on actual earthquake performance. However, a considerable amount of analytical and experimental research from countries including Japan, Iran, Turkey, Canada, the United Kingdom, and the United States, has been undertaken since the early 1970s, the bulk of which has occurred over the last ten years. The consensus of this body of research is that the system is ductile and has good energy dissipation capacity, and is cost effective as both a new building lateral system and as a potential retrofit scheme. SPSW systems do however require a little more effort to model and analyze correctly when compared to some of the other commonly adopted lateral systems, and the design process often requires many iterations. Figure A shows schematically the load paths within a typical SPSW.

1.2 Web Plate Behavior

The web plate is the main lateral force resisting component of the SPSW, and since elastic shear buckling occurs at very low load levels, is permitted to resist lateral load in the post-buckled state primarily by diagonal tension field action. Under monotonic loading the web plate has strength and stiffness compatible with the conventional assumption of a pure tension field. Under cyclic loading, web plates have been shown to have considerable ductility capacity, although the hysteresis can be severely pinched. The AISC Seismic Provisions for Structural Steel Buildings require the designer to size the web plate to resist the entire story shear.

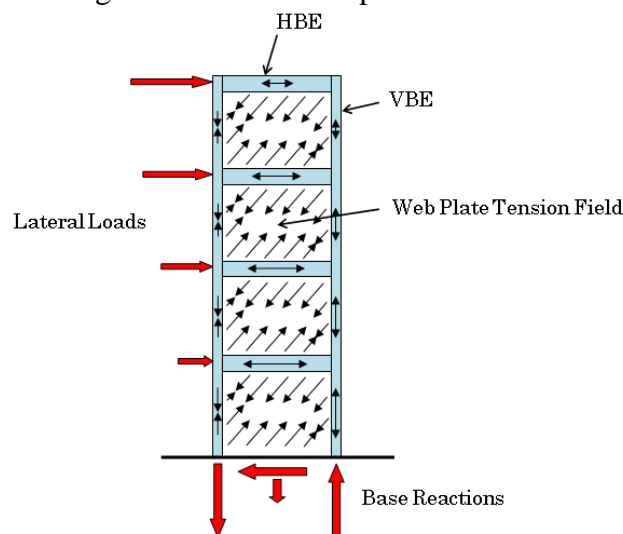


Figure A: Typical SPSW showing load paths

1.3 Vertical Boundary Elements

The vertical boundary elements act in much the same way a plate girder flange does, by anchoring the web plate tension field. The VBEs must have sufficient strength and stiffness to allow the tension field to fully develop plastic over-strength and they must remain entirely elastic in the process. The VBEs are subjected to forces resulting from frame action and from web plate pull-in. In design, these sources of loading are often considered separately when determining VBE demand.

1.4 Horizontal Boundary Elements

The horizontal boundary elements act as struts that resist web-plate pull-in forces and transfer a large portion of the total lateral load from the floors above to the wall below.. HBEs also resist vertical out-of-balance loading resulting from differences in web plate strength above and below. HBEs are permitted to form plastic hinges at the ends, much like a moment frame, but must be designed to avoid hinging over the span.

1.5 Overview of this Document

The research presented in this document reports on computational analyses carried out using the general finite element platform ABAQUS. The focus of this study is on the elastic and inelastic post-buckling behavior of SPSW web plates under monotonic loading and how this behavior affects the force demands on the VBEs, and conversely how the VBE properties influence the behavior of the web plate. This interaction is important for understanding the performance of the SPSW system. Three interrelated aspects of SPSW web plate-boundary frame interaction will be examined and the results contrasted with the generally accepted practice in SPSW design.

1.5.1 VBE Stiffness

The first concerns a requirement in both the Canadian (CSA 2009) and US codes (AISC 2010) that the VBE flexural stiffness exceed a prescribed minimum value, which is a function of the height, length and thickness of the web plate. The minimum I_c required by the Provisions is:

$$I_c = 0.0031t_w h^3 / L \quad (1)$$

The minimum VBE stiffness was introduced into the code out of concern that adequate system ductility be provided (Lubell 2000). The VBEs must have stiffness sufficient to anchor the web plate and enable a uniform stress field to develop. If the VBEs are too flexible the stress field will be highly non-uniform and plasticity will be concentrated only in certain regions of the web plate. The original analysis was based on an idealized elastic plate girder and is accordingly limited. Although the analysis is extended to seismic response prediction of SPSWs, it is not consistent with many aspects peculiar to the SPSW system. Furthermore, although the established threshold for stress field uniformity ultimately embedded in the code equation is reasonable, it was established somewhat arbitrarily and has since been found to be uncorrelated with available test data (Qu 2008).

1.5.2 Tension Field Inclination

The second aspect addressed in this paper concerns a requirement in the AISC Provisions for determining the orientation of the web plate tension field, typically referred to in the literature as the angle α , and measured from the vertical. The equation (F5-2 in the provisions) is repeated here for convenience.

$$\tan^4 \alpha = \frac{1 + \frac{t_w L}{2A_c}}{1 + t_w h \left(\frac{1}{A_b} + \frac{h^3}{360I_c L} \right)} \quad (2)$$

Where A_b and A_c are the cross-sectional area of the HBE and VBE respectively, I_c is the VBE moment of inertia, t_w is the panel thickness, L is the distance between VBE center-lines and h is the distance between HBE center-lines.

In capacity design, α is used to compute force demands on the boundary elements and lateral strength of the plate. The original derivation for this equation was also based on an elastic analysis and employed the principle of least work. The angle is computed for the various stages of loading in the computational models and compared with the code equation.

1.5.4 VBE Demand From Web Plate Pull-in

In conventional design, the force demands on the VBEs resulting from web-plate pull-in are computed using $R_y F_y t_w \sin^2(\alpha)$, where α is derived from Eq. 2 (or 40°) and $R_y F_y$ is the expected yield strength of the web plate, which does not include strain hardening. This demand on the VBEs is compared and contrasted with the results of the simulations.

1.6. Elastic Shear Buckling of Rectangular Plates

The classical solutions for elastic shear buckling of thin plates have been presented by many researchers exploring the behavior of SPSW web plates and will not be presented here in detail. For this study, the critical buckling stress (τ_{cr}) is based on pure elastic shear buckling of a rectangular plate with clamped edges and a rigid boundary. It can be expressed as follows:

$$\tau_{cr} = K \frac{E}{1 - \nu^2} \left(\frac{t}{b} \right)^2 \quad (3)$$

Curve fitting tabular data (Young 1989) for the parameter K yields:

$$K = 7.38 + 5.32 \left(\frac{b}{a} \right)^{1.33} \quad (4)$$

Where a and b are respectively the long and short dimensions of the plate, and t is the plate thickness.

2. Computational Modeling (ABAQUS)

The ABAQUS model developed for this study was devised so that several phenomena could be examined, with particular attention focused on the web plate and the VBE behavior. The model

represents an arbitrary single story sub-assembly of a multi-story SPSW, with WF HBE and VBE sections. The HBEs are moment connected to the VBEs, as is required by the Provisions. The HBE and VBE sections are determined so that, for a prescribed geometry, the members satisfy the strength and compactness requirements of the Provisions. The HBE section A_g and Z_x are set to half of that required for a continuous SPSW system. In this way the HBE will deliver a similar flexural demand to the VBEs, as would occur for a continuous system with an equal panel thickness and story height above and below. The halving of A_g accounts for the absence of plate pull-in force contribution from the adjacent story. Therefore the axial shortening of the HBE in the model will be compatible with a continuous system. The geometry can be modified to suit a prescribed bay length (L), story height (h), web plate thickness (t_w), boundary element section properties and applied moment-shear demand ratio (M_{OT}/V). Neither dead nor live loads were included in the analyses.

2.1 Boundary Conditions and Constraints

Special care was taken to model the boundary conditions so that they approximate, as closely as possible, the boundary conditions in a continuous wall system. To approximate the effect of having continuous VBEs through the beam-column joint, the top and bottom of each VBE are constrained to have equal in-plane rotation. The VBEs are otherwise free to rotate and translate. The HBEs are rigidly connected to the VBEs with a half column depth offset that maintains normality. VBE panel zone flexibility is not modeled. The mid-point of both the top and bottom HBE is constrained to lie on a straight line between opposite ends of the HBE member. This ensures that the HBE can flex near the ends where moment demand is typically highest, can shorten axially, but it is restrained from deflecting vertically at mid-span. This constraint attempts to capture the axial and localized flexural demands on the HBE without permitting excessive center span deflection for cases of large HBE span-depth ratios, which would influence the web-plate stress field. In a real system the HBE is largely (though not entirely) prevented from deflecting vertically by the presence of the web plate in the adjacent story. The left VBE bottom node is pinned while the right VBE bottom node has a roller boundary condition. The boundary conditions and kinematic constraints are shown in Figs. 1 and 2.

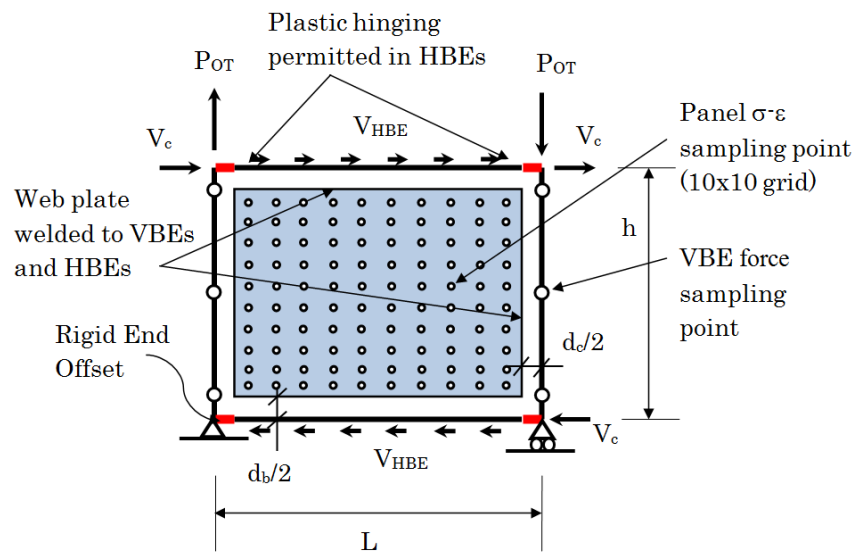


Figure 1: Generic ABAQUS Model Template.

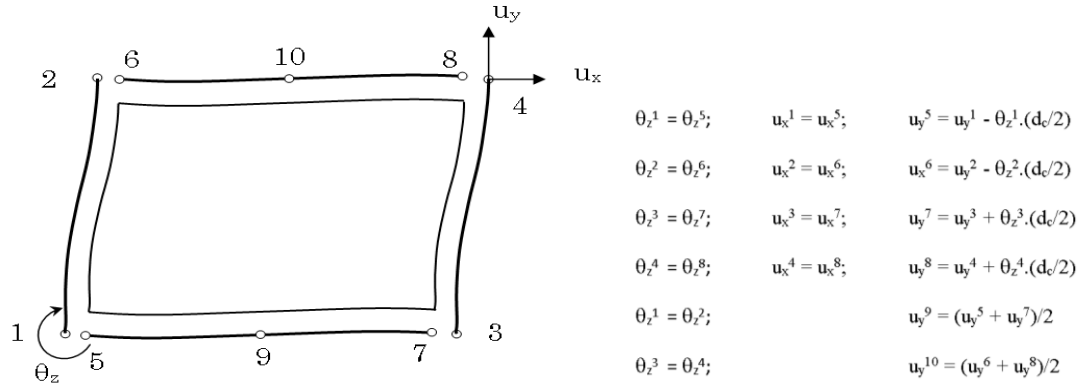


Figure 2: ABAQUS Model Kinematic Constraints.

2.2 Selection of Model Parameters

To examine the effect of VBE slenderness, two suites of models were analyzed; one suite comprised flexurally slender VBE sections (limited to W12 or W14), the other with deeper and typically lighter sections (limited to W24 through W40). For the first suite, and for a given geometry, the most flexurally slender section was adopted for the model, regardless of whether or not the VBE satisfied the AISC minimum stiffness limit. As previously discussed, this was done to examine this particular provision. For the second suite of models, the most efficient section (by weight) was selected.

Designs were selected to satisfy capacity design requirements for various M_{OT}/V ratios and the resulting designs are in shown in Table 1.

Table 1 - Sub-Assembly BE Sizes and Panel Geometry

Assm #	VBE	HBE	(m) L	(m) h	(mm) tw	(m) MonV	(Eq. H1-1) AISC Int	β	(deg) AISC α
1	W14X730	W30X211	5.69	6.15	9.5	24.3	0.984	0.81	37.26
2	W14X730	W30X235	4.88	6.1	8.1	24.3	0.962	0.83	37.74
3	W14X605	W21X111	4.57	5.72	3.8	12.1	0.956	1.63	38.78
4	W14X605	W27X178	4.57	5.72	5.1	6.0	0.983	1.22	38.92
5	W14X550	W24X146	3.66	4.57	6.1	12.1	0.998	1.74	39.15
6	W14X500	W27X178	3.66	4.57	6.1	6.0	0.964	1.51	39.52
7	W14X370	W24X146	3.66	4.57	4.1	24.3	0.967	1.50	39.89
8	W14X500	W21X93	4.57	4.35	3.8	24.3	0.973	3.68	40.05
9	W14X665	W36X256	5.49	5.23	6.1	6.0	0.956	2.01	40.59
10	W14X455	W27X194	4.57	4.35	5.1	6.0	0.983	2.42	41.06
11	W14X665	W24X146	6.4	4.13	5.3	12.1	0.995	6.87	41.23
12	W14X730	W36X302	6.4	4.92	7.1	12.1	0.963	2.94	41.44
13	W14X665	W40X278	6.4	4.92	5.3	24.3	0.962	3.40	41.86
14	W14X605	W40X264	6.4	4.13	5.3	6	0.991	5.98	42.68
15	W36X800	W21X122	3.66	4.57	6.1	24.3	0.971	11.93	39.64
16	W27X539	W30X211	5.49	5.23	9.1	6.0	0.976	2.77	39.99

Table 1 - Cont. Sub-Assembly BE Sizes and Panel Geometry

Assm #	VBE	HBE	(m) L	(m) h	(mm) tw	(m) MonV	(Eq. H1-1) AISC Int	β	(deg) AISC α
17	W36X652	W30X211	6.4	6.1	7.1	24.3	0.986	4.43	40.32
18	W36X487	W30X211	6.4	6.1	7.1	12.1	0.963	3.15	40.43
19	W30X261	W18X86	3.66	4.57	3	12.1	0.978	4.83	40.68
20	W33X387	W24X146	4.57	5.72	3.8	24.3	0.985	3.67	40.75
21	W36X800	W36X256	6.4	4.92	10.7	24.3	0.964	8.87	40.88
22	W40X372	W27X178	3.66	4.57	6.1	6.0	0.991	5.46	41.15
23	W30X211	W21X111	3.66	4.57	3.0	6.0	0.971	3.80	41.36
24	W36X395	W24X146	4.57	4.35	5.1	6.0	0.971	9.58	41.48
25	W27X539	W36X256	5.49	5.23	6.1	12.1	0.955	4.15	41.6
26	W40X593	W24X146	6.4	4.13	5.3	12.1	0.972	27.92	41.71
27	W40X593	W36X256	6.4	6.1	5.3	12.1	0.997	5.88	41.73
28	W36X487	W40X278	6.4	6.1	5.3	6.0	1	4.2	41.90
29	W36X652	W40X264	6.4	4.92	7.1	12.1	0.983	10.40	42.06
30	W40X503	W36X256	6.4	4.13	10.7	12.1	0.995	11.52	42.29
31	W36X361	W24X162	5.49	4.22	4.6	24.3	0.966	13.05	42.43
32	W36X487	W27X235	6.4	4.92	5.3	24.3	0.966	9.87	42.51
33	W40X503	W36X302	6.4	4.92	7.1	6.0	0.99	8.55	42.67
34	W40X431	W36X256	5.49	4.22	6.1	6.0	0.984	13.26	42.98
35	W36X487	W40X294	6.4	4.13	7.1	24.3	0.994	14.96	43.27

The VBE flexibility ratio (β), defined for this study as I_c provided divided by I_c required by Eq. 1, ranged from 0.81 to 27.9, with a mean of 6.3. Two of the thirty-five combinations had a β less than unity.

2.3 Load Application

The loads shown on Fig. 1 were applied proportionally using a smooth ramp function designed specifically for these analyses. The duration of the load application and the magnitude of the applied loads depend on the member sizes, plate thickness and panel geometry. An estimate of this load is made prior executing each analysis to optimize the solution time.

The lateral loads are applied to the tops of the VBEs as concentrated point forces and to the top HBE as a uniformly distributed force. The forces are approximately proportional to the share of lateral load resisted by the boundary frame and web plate from a plastic analysis. A point force is applied to the bottom of the right VBE. It is equal in magnitude to the force applied to the tops of the VBEs, but opposite in direction. A uniformly distributed force equal in magnitude to that applied to the top HBE is applied to the bottom HBE, also in the opposite direction. In this way the reaction force at the bottom left VBE will be approximately equal in magnitude to the point force applied to the bottom of the right VBE, thus maintaining symmetry.

2.4 Web Plate

The ABAQUS S4R element (ABAQUS 2009) was used to model web plates and has been used successfully by many researchers (Habashi 2011). This element is a four-noded doubly curved, reduced integration shell element with finite strain, large rotations and hourglass control. Nine Gauss points were used through the thickness of the shell to accurately capture inelastic out-of-plane bending behavior of the web plate. Some researchers (Habashi 2011) have found that a

minimum of thirty elements along a panel edge are required to obtain adequate convergence, so this was adopted as a minimum. Many others have used fewer elements with satisfactory results. The material model for the web plate is elastic-perfectly plastic A36 steel ($R_y F_y = 372$ MPa; $E = 205,000$ MPa).

2.5 Boundary Frame Elements

The boundary frames were modeled using the B31 shear deformable beam element. This element is a two-node, general purpose beam element with finite strain, large rotation capability and a single centrally located integration point. Section properties are determined and maintained before the analysis. The HBEs are modeled with bilinear material properties, approximating A572 Gr 50 steel ($R_y F_y = 379$ MPa; $E = 205,000$ MPa; and $E_{sh} = 0.004E$). The HBEs are moment connected to the VBEs. The VBEs are modeled as elastic B31 elements and are not permitted to yield. The analysis includes full geometric nonlinearity. Since the VBEs were capacity designed, yielding was not expected to occur and VBE demands were checked against those used in the selection process.

2.6 Initial Imperfections

The web plates were modeled with an initial imperfection comprising bi-harmonic functions, with the following form:

$$z(x, y) = \sum_{n=1}^3 A_n \sin\left(\frac{n\pi x}{L}\right) \sin\left(\frac{n\pi y}{h}\right) \quad (5)$$

For all of the analyses, the maximum amplitude of the resultant imperfection was set to approximately 7 mm out of the plane of the web plate. The HBEs and VBEs were not modeled with initial imperfections.

2.7 Solution Strategy

All of the analyses were performed using the ABAQUS Explicit solver, which has been used successfully by other SPSW researchers (Behbahanifard 2003). This solver uses a dynamic time stepping explicit solution strategy for displacement updating and is generally advantageous for very short duration transient dynamic analysis and contact problems, but can also be used successfully for quasi-static processes.

2.8 Web Plate Stress and Strain Sampling

For reasons of post-processing efficiency, the web plate field variables were not recorded at each element, but on an evenly spaced ten-by-ten grid (See Fig. 1). The density of the grid could be altered and was done so to test the sensitivity of the results to changes in the number of points sampled. A ten-by-ten grid was found to be sufficient for this purpose. Field variables were recorded at a maximum of one-hundred evenly spaced time increments. The stress components, σ_{11} , σ_{22} , and σ_{12} and the equivalent plastic strain ϵ_{PEEQ} were recorded at each time increment. A post-processing algorithm was used to compute the principal stress components and the orientation of these components. For each of the variables sampled and at each time increment, the mean, standard deviation and coefficient of variation were also computed.

2.9 VBE force sampling

The shear force, axial force and bending moment demands for the VBEs were recorded at the top, bottom and mid-span of the member. These quantities were recorded at the same sampling rate as for the web plate. The total equivalent bending moment M_{eq} and the total lateral pull-in force V_{eq} were computed from the ABAQUS output and compared with the corresponding values generated assuming a pure tension field with the inclination angle (α) set to the code mandated value. The total equivalent bending moment and lateral force are defined as follows:

$$M_{eq} = \frac{1}{2}(M_{top} + M_{bot}) - M_{mid} \quad (6)$$

$$V_{eq} = \frac{1}{2}(V_{top} - V_{bot}) \quad (7)$$

These quantities are used to assess the magnitude of the bending and shear force demands on the VBEs resulting only from the pull-in force delivered by the web plate.

3. Discussion of Simulation Results

Below is a brief discussion of the key simulation results. Since many different sub-assembly geometries were modeled, the analysis of the results lends itself to some statistical treatment. It is worth reiterating that the results pertain only to a single quarter cycle of monotonically increasing load and that direct application to reversed cyclic loading is not strictly appropriate and needs further study; it does however serve as a baseline for cyclic analyses.

3.1 VBE AISC Capacity Check

The VBE forces were extracted from the simulations at 2% drift and the capacities checked using the AISC interaction equations to validate the used of elastic member properties. The mean value of member interaction for all of the assemblies was computed to be 1.069, slightly higher than the code limit of 1.00, but probably still within the realm of substantially elastic behavior.

3.2 Elastic Critical Load Analysis

An eigen-value analysis was performed on each assembly (with zero web plate imperfection) and the shear stress at buckling (τ_{cr}) extracted to validate the closed form solution represented by Eq. 4. The elastic critical stress was used for comparison with the observed stress field at various stages of loading.

The ratio of the elastic critical buckling stress computed using ABAQUS to that of Eq. 4 is observed to be approximately 1.125 (SD = 0.094). The magnitude of τ_{cr} computed from the eigen-value analysis varied from a minimum of 2.2 MPa to a maximum of 25.7 MPa, with a mean of 7.2 MPa. Considering the broad scatter of critical stresses observed for these assemblies and the differences between the closed form solution and the ABAQUS model, the correlation between the simulation and Eq. 4 is very good.

Examination of the stress field development in the pushover analyses of each assembly reveals a point at which buckling appears to initiate. Since the plates are modeled with an initial

imperfection, the actual buckling stress is not directly observable from the stress field. There is however typically an obvious transition from pre-buckling to post-buckling behavior (See Fig. 4). This stress state, referred to here as the *apparent* critical shear stress, is computed for each of the assemblies and occurs when magnitude of the mean principal compressive stress drops below 95% of the mean principal tensile stress.

3.3 Web Plate Stress Field Development

Regardless of the assembly geometry or applied loads, the web plate stress field developed in a consistent manner for each of the assemblies analyzed. Prior to elastic buckling, the magnitude of both the mean principal tensile stress ($|\sigma_{pt}|$) and the mean principal compressive stress ($|\sigma_{pc}|$) increase almost at the same rate, and the plate is subjected to a state of pure in-plane shear with the principal stresses being oriented at close to 45 degrees. As the lateral load continues to increase $|\sigma_{pc}|$ diverges abruptly from $|\sigma_{pt}|$, signifying buckling. This apparent buckling shear stress (τ_{app}) is consistently higher than that predicted by elastic critical load analysis. Fig. 3 shows the relationship between $|\sigma_{pc}|$ and $|\sigma_{pt}|$ for assembly #6.

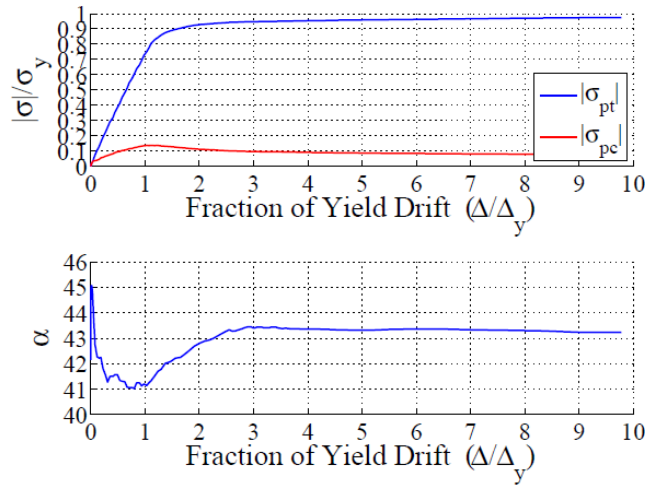


Figure 3: Mean principal stress magnitudes normalized by σ_y (σ/σ_y), and mean tension field orientation (α) determined from ABAQUS: Assembly # 6 with W14X500 VBEs; W27X178 HBEs; L = 3.66 m; h = 4.57 m; t_w = 6.1 mm.

Fig. 4 shows the relationship between $|\sigma_{pc}|$ and $|\sigma_{pt}|$ for assembly #6 just as the plate appears to buckle. Also shown on this plot is the elastic critical load. Fig. 5 shows the relationship between τ_{app} and the actual elastic critical stress τ_{cr} plotted against plate D/t ratios. From this plot it is clear that the capacity of a very thin plate to resist in-plane compressive stress may significantly exceed the compressive stress associated with elastic shear buckling. This occurs because, in the presence of out-of-plane buckling deformations, the membrane tensile stresses must be anchored by membrane compressive stresses in regions of high synclastic curvature (double curvature of the same sign) even if the plate has negligible out-of-plane bending stiffness. This high curvature occurs at the plate boundaries and diminishes towards the center of the plate.

After buckling, $|\sigma_{pc}|$ increases with additional drift and reaches a maximum value $|\sigma_{pc,max}|$ when the drift is between 1.0 and 1.3 times the yield drift (mean = 1.16 Δ_y ; SD = 0.08 Δ_y for all assemblies). As the drift continues to increase beyond $|\sigma_{pc,max}|$ it reduces and asymptotically approaches a residual magnitude $|\sigma_{pc,res}|$, which is $|\sigma_{pc}|$ at 2% drift. For a given E and σ_y , the $|\sigma_{pc}|$ attained at the various stages of loading appears to be primarily a function of span-to-thickness ratio and is consistently higher than τ_{cr} . The span being defined here as the minimum of L and h , and designated here as D . Fig. 7 shows the magnitude of $|\sigma_{pc}|/\sigma_y$ at drifts of Δ_y and 2% for a range of plate D/t ratios.

Though the effect of this residual stress was identified by SPSW researchers (Roberts 1991) some two decades ago, in this case by assuming τ_{cr} is maintained after elastic buckling, it has largely been ignored by the SPSW research community. Others have included a compression brace (Shishkin 2005) to account for the compressive resistance of the web plate, but this particular model captured only the global effect on total story strength and stiffness, not the interaction with the VBEs. More recently, researchers have accounted for it by including τ_{cr} in the development of hysteretic models (Choi 2010). As was just pointed out, τ_{cr} generally underpredicts $|\sigma_{pc,res}|$. However, Choi investigated the hysteretic behavior of a relatively thick plate with an h/t of 375. The ratio of $|\sigma_{pc}|$ to τ_{cr} for this span-thickness ratio was found to be (in the present study) approximately 1.5. As D/t increases this ratio can exceed 10. Fig. 6 shows how the computed $|\sigma_{pc,res}|$ is related to τ_{cr} for different D/t ratios.

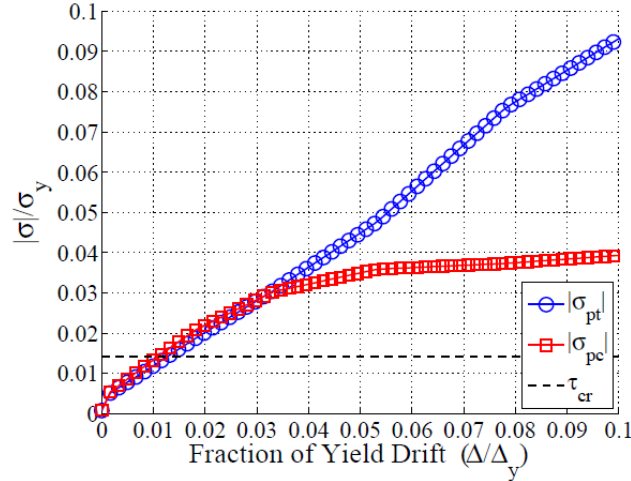


Figure 4: Principal stress magnitudes v's drift for Assembly #6 showing computed τ_{cr} from elastic critical load analysis

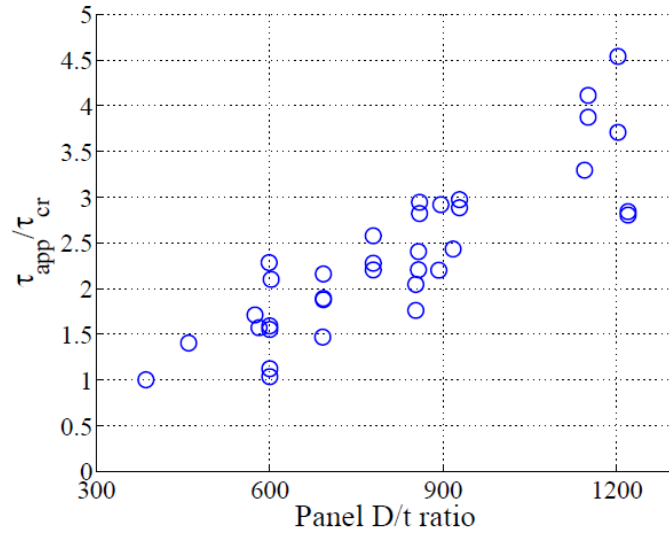


Figure 5: Ratio of observed buckling shear stress (τ_{app}) and ABAQUS computed τ_{cr} for different D/t ratios

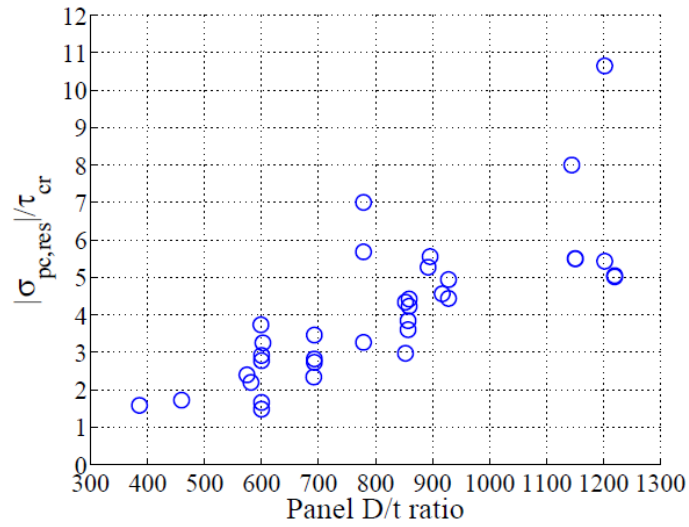


Figure 6: Ratio of residual mean compressive stress magnitude ($|\sigma_{pc,res}|$) to ABAQUS computed τ_{cr} for different D/t ratios.

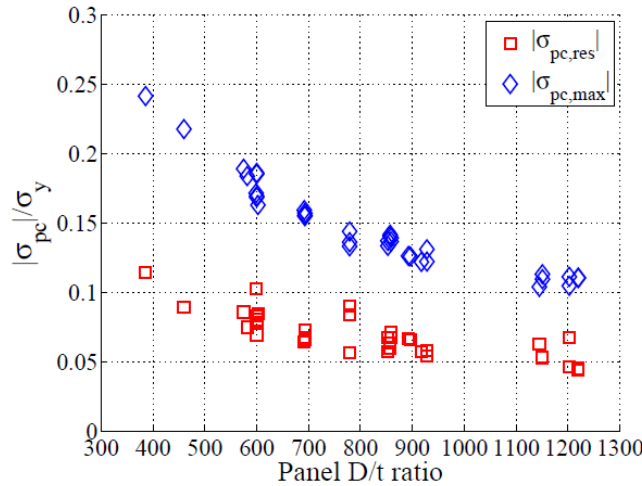


Figure 7: Mean compressive stress magnitude ($|\sigma_{pc}|$) in web plate for different D/t ratios. (normalized by yield stress σ_y)

3.3.1 Influence of VBE Flexibility on Stress Uniformity and Plastic Strain.

The influence of VBE flexibility on the web plate ductility demand is explored using two metrics: **a)** the coefficient of variation of the principal tensile stress ($C\sigma_{pt}$) prior to significant yielding, and **b)** the coefficient of variation of the mean equivalent plastic strain ($C\varepsilon_{PPEQ}$) at 2% drift.

Fig. 8 shows $C\sigma_{pt}$ plotted against β at drifts of $0.5\Delta_y$ and Δ_y , respectively. At $0.5\Delta_y$, assembly #1 and #2 (both with β values less than unity) have a $C\sigma_{pt}$ of 0.28 and 0.32 respectively; significantly above the mean value of 0.22 (with $SD = 0.028$). The situation is similar, although slightly less obvious, when the drift is at Δ_y with $C\sigma_{pt}$ values of 0.26 and 0.27 (mean = 0.20, $SD = 0.025$). For assemblies with $\beta > 1$, there appears to be no relationship between β and the uniformity of the stress field. This observation is consistent with the code provision, and with expectation.

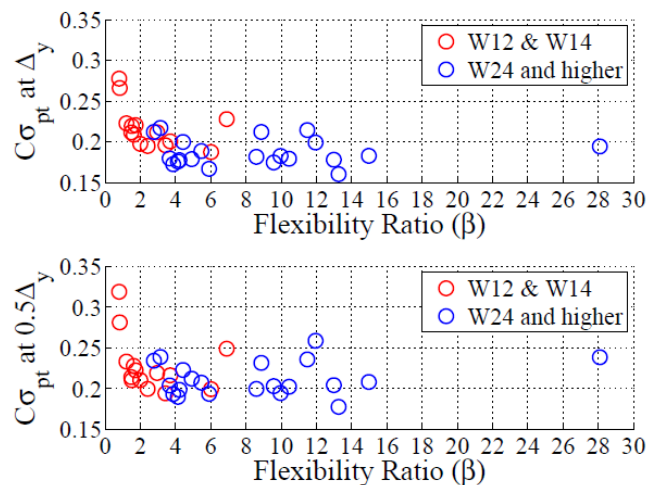


Figure 8: Relationship between flexibility ratio β and the measured $C\sigma_{pt}$ in web plate at $0.5\Delta_y$ and at Δ_y .

Fig. 9 shows the relationship between $C_{\mathcal{E}_{PPEQ}}$ and β at a drift of 2%. At this drift level there has been significant plastic strain throughout the plate, variations in membrane stresses have been largely eliminated and plastic strain demands are evening out. There is no observable trend in this data and statistical analysis reveals the same. Interestingly, the $C_{\mathcal{E}_{PPEQ}}$ for assembly #1 and #2 are below the mean of the group, signifying that for this measure of ductility demand the low β value had no impact on the uniformity of the plastic strains.

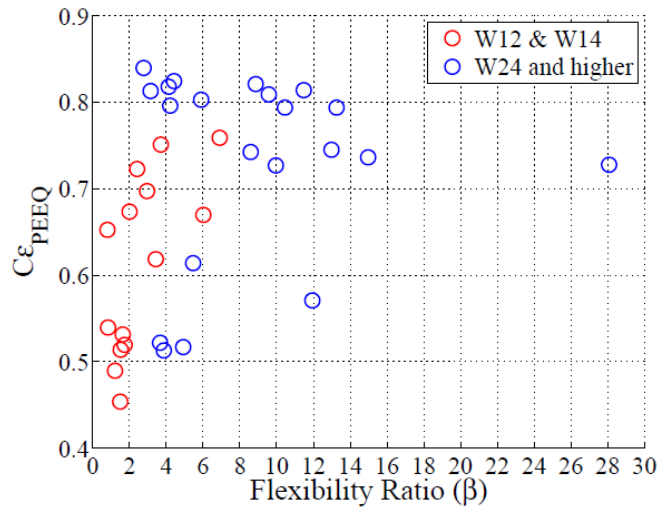


Figure 9: Relationship between flexibility ratio β and the measured $C_{\mathcal{E}_{PPEQ}}$ in web plate at Δ_y .

3.4 Tension Field Inclination Angle

The orientation of the tension field for each of the assemblies was computed and recorded at the end of each time increment. The relationship between the predicted inclination angle using the AISC equation (α_{AISC}) and the angle predicted by ABAQUS (α_{ABQ}) is shown in Fig. 10. This figure presents the correlation between the two at yield drift, where α is close to the minimum value, and at 2% drift where the web plate is completely plastic. It is clear that there is a relationship between the α_{AISC} and α_{ABQ} in the elastic range, although α_{ABQ} is consistently closer to 45 degrees. However, in the fully plastic condition the correlation completely breaks down and no relationship appears to exist (correlation coefficient = 0.0071). The mean α_{ABQ} at 2% drift for the thirty-five assemblies was computed to be 43.4 degrees.

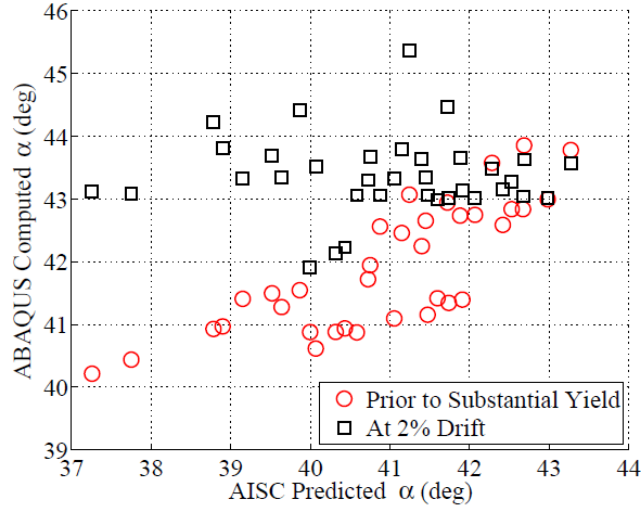


Figure 10: Correlation between α predicted by AISC equation and α predicted by ABAQUS.

One significant consequence of this is apparent when computing peak lateral pull-in forces on the VBEs, as is required for capacity design procedures. In seismic design, the use of α_{AISC} may under certain circumstance significantly under-predict the lateral forces on the VBE. To illustrate this point, consider the case where α_{AISC} is computed to be 37 degrees. Since the lateral force is a function of $\sin^2 \alpha$, the ratio between the “actual” and computed lateral force (assuming a pure tension field) is $\sin^2(43.4^\circ)/\sin^2(37^\circ) = 1.30$.

It should be pointed out that this lateral force is not the only source of bending and shear forces in the VBEs; frame action accounts for a substantial portion of the net effect. Furthermore, the presence of membrane compressive stresses alleviate this apparent overload condition to a considerable degree. This will be discussed in the next section.

3.5 VBE Demand from Web Plate Pull-in

The VBE member forces from web plate pull-in are determined by using Eqs. 6 and 7. From these bending moments and shear forces it is possible to determine equivalent distributed lateral forces on the VBEs, denoted w_{eq} . For the present study, only the VBE bending moments will be used to determine w_{eq} . By including the mean compressive membrane stress which acts with the tensile stress, and the actual tension field inclination angle, α_{act} , the lateral load at the web plate-VBE boundary may be computed using the following equation:

$$w_{est} = (|\sigma_{pt}| \sin^2 \alpha_{act} - |\sigma_{pc}| \cos^2 \alpha_{act}) t_w \quad (8)$$

Where w_{est} is the lateral force estimated using the mean compressive and tensile membrane stresses in the plate. The seismic provisions require that α be computed using Eq. 2, or 40 degrees. For comparison, the effective lateral force using α computed from Eq. 1 (w_α) and using 40 degrees (w_{40}) are included in the following three plots. Both of these are used in conjunction with a pure tension field stress of R_y times F_y (σ_y). Figs. 10, 11 and 12 show each of these lateral force estimates normalized by a pure tension field with magnitude $R_y F_y t_w$ operating at 45 degrees

(w_{45}). Fig. 11 is for the case where the drift is at Δ_y , or approximately 0.3 to 0.4%. Fig. 12 shows the same relationship at a drift of $2\Delta_y$. Fig. 13 is at 2% drift.

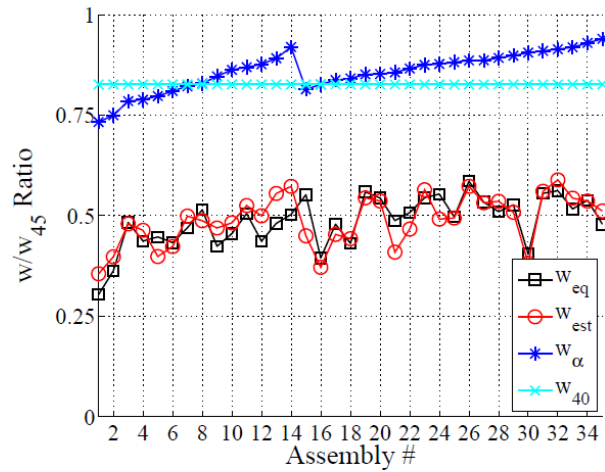


Figure 11: Lateral load delivered to VBE by web plate at Δ_y using different estimates (normalized by plastic tension field oriented at 45 degrees)

It can be concluded from Fig. 11 that at moderate drift levels (at or below the theoretical yield drift) the code based equation may significantly over-predict the lateral pull-in force of an elasto-plastic web plate. The same occurs at $2\Delta_y$, though to a lesser extent. The lateral load, w_{est} , estimated using Eq. 8 matches quite well the equivalent load, w_{eq} , determined from the member bending moments. It can be concluded from this analysis that although the compressive membrane stresses are highly variable for the entire drift history (SD often exceeding the mean), the average field value provides a reasonable estimate of the compressive stress at the vertical boundaries and a reliable basis for computing lateral forces on the VBEs. Since the average compressive stress is quite stable and relatively easy to predict (for this loading regime) it would be prudent and perhaps advantageous to account for it.

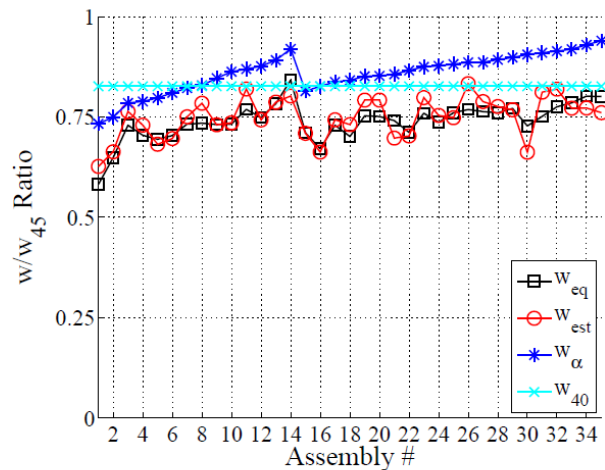


Figure 12: Lateral load delivered to VBE by web plate at $2\Delta_y$ using different estimates (normalized by plastic tension field oriented at 45 degrees)

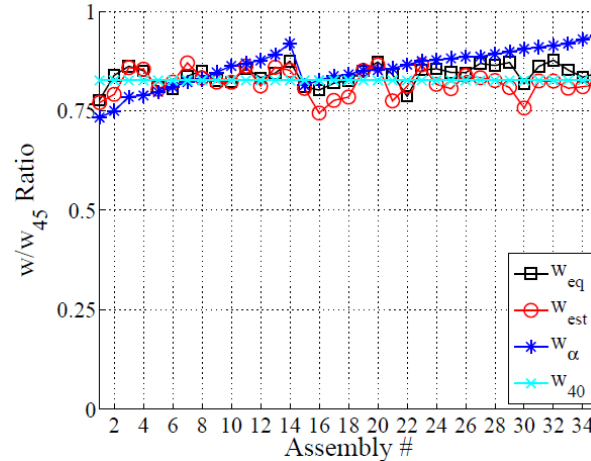


Figure 13: Lateral load delivered to VBE by web plate at 2% drift using different estimates (normalized by plastic tension field oriented at 45 degrees)

At 2% drift, the three estimates yield a similar result. The load deduced using the AISC alternate α of 40 degrees (w_{40}) does a better job of matching the model than Eq. 2.

4. Summary and Conclusions

The key observations and conclusions from these analyses are summarized below. All of these are made in the context of monotonic loading on a subsystem with an elastic-perfectly plastic web plate. Any extrapolation to cyclic loading with hardening is not appropriate without additional research.

- The inclination of the web plate elastic tension field (α) has a tendency to be closer to 45 degrees than the ASIC equation predicts. The difference is more pronounced as the AISC predicted angle gets smaller.
- For systems that have an initial tension field inclination less than 45 degrees, α approaches 44 degrees at large drifts, regardless of its initial elastic value. The majority of this shift occurs within approximately two times the yield drift.
- For a broad range of VBE stiffnesses, the flexibility parameter β has a noticeable influence on the uniformity of the elastic principal tensile stresses in the web plate when drifts are low (less than yield drift).
- For a broad range of VBE stiffnesses, the flexibility parameter β has no bearing on the uniformity of plastic strains in the web plate when the drifts are large ($> 2\%$).
- The elastic critical load (τ_{cr}) does not, by itself, adequately predict either the mean peak or mean residual compressive stresses that develop in the web plate. These stresses appear to be a function of the web plate span-thickness ratio and a simple relationship can be established. These stresses may also be a function of web plate yield stress, although this was not examined.
- When drifts are less than two times the theoretical yield drift, the mean tensile stress, mean compressive stress, and the mean α can be used to accurately predict VBE bending demands. This may have implications for non-seismic driven design.

- At high drifts ($> 2\%$), the AISC alternate α (40 degrees) more accurately predicts the bending demand on the VBEs than the AISC elastically derived α .

Acknowledgments

Financial support for this study was provided by the National Science Foundation as part of the George E. Brown Network for Earthquake Engineering Simulation under award number CMMI-0830294. Any opinions, findings, conclusions, and recommendations presented in this paper are those of the authors and do not necessarily reflect the views of the sponsors.

References

- ABAQUS. (2009). ABAQUS User's Manual. Version 6.9: Dassault Systèmes Simulia Corp. Providence, RI, USA.
- AISC (2010). "Seismic Provisions for Structural Steel Buildings." ANSI/AISC 341-10, American Institute of Steel Construction, Inc., Chicago, IL.
- AISC (2010) "Specification for Structural Steel Buildings". ANSI/AISC 360-10, American Institute of Steel Construction, Inc., Chicago, IL.
- Behbahanifard M.R. (2003). "Cyclic Behavior of Unstiffened Steel Plate Shear Walls". *PhD Dissertation*, University of Alberta, Canada
- CSA. (2009). "Design of Steel Structures." CAN/CSA S16-09, Canadian Standards Association, Mississauga, ON, Canada.
- Choi I., Park H. (2010) "Hysteresis Model of Thin Infill Plate for Cyclic Nonlinear Analysis of Steel Plate Shear Walls". *ASCE Journal of Structural Engineering*, Nov. 1423-1434
- Habashi H.R., Alinia M.M. (2011). "Characteristics of the wall-frame interaction in steel plate shear walls". *Journal of Constructional Steel Research*, Department of Civil Engineering, Amirkabir University of Technology, Tehran, Iran.
- Kaufmann E.J., Metrovich B., Pense A.W. (2001). "Characterization of Cyclic Inelastic Strain Behavior On Properties of A572 Gr. 50 and A913 Gr. 50 Rolled Sections". *ATLSS Report No. 01-13*, Lehigh University.
- Lubell A. S., Prion, H.G.L., Ventura C.E., Rezai M., (2000). "Unstiffened Steel Plate Shear Wall Performance Under Cyclic Loading". *Journal of Structural Engineering*, 126(4) 453-460
- Qu B., Bruneau. M (2008). "Seismic Behavior and Design of Boundary Frame Members of Steel Plate Shear Walls". *Technical Report MCEER-08-0012*.
- Roberts T.M., Ghomi S.S. (1991). "Hysteretic Characteristic of Unstiffened Plate Shear Panels". *Thin Walled Structures* (12) 145-162.
- Sabouri-Ghomi S., Ventura C.E., Kharrazi H.K., (2005) "Shear Analysis and Design of Ductile Steel Plate Walls". *ASCE Journal of Structural Engineering*, (6) 878-889.
- Shishkin J.J., Driver R.G., Grondin G.Y. (2005) "Analysis of Steel Plate Shear Walls using the Modified Strip Model". *Structural Engineering Report No. 261*, University of Alberta, Canada.
- Young, W.C. (1989). "Roark's Formulas for Stress and Strain. 6th Edition" *McGraw Hill International*.